Precise 3D Deep Brain Stimulation Electrode Location based on Multimodal Neuroimage Fusion

Nádia Moreira da Silva[1], Verena E. Rozanski[2], Sérgio Neves Tafula[1] and João Paulo Silva Cunha[1,3]

[1]INESC TEC (Instituto de Engengaria de Sistemas e Computadores do Porto), University of Porto,
Rua Roberto Frias 4200-465, Porto, Portugal
[2]Department of Neurology, University of Munich at Marchioninistrasse 15, 81377 Munich, Germany
[3]Faculty of Engineeiring, University of Porto, Rua Roberto Frias 4200-465, Porto, Portugal

Keywords: DBS, Parkinson, Dystonia, Co-registration, Electrodes Segmentation.

Abstract: The success of neurosurgery strongly depends on the pre-neurosurgical evaluation phase, in which the delineation of the areas to be removed or to be stimulated must be very accurate. For patients undergoing Deep Brain Stimulation (DBS) it is vital the delineation of the target area prior to surgery, and after the implantation of the DBS lead to confirm the electrodes positioning. In this paper we present a system to accurately determine the 3D position of DBS electrodes implanted within the brain of Parkinson and Dystonia patients. The system was tested using a multimodal dataset from 16 patients (8 with Parkinson`s disease and 8 with dystonia) and, on average, the differences between the detected electrodes positions and the ones estimated manually by an experienced physician were less than a voxel in all cases.

1 INTRODUCTION

Movement disorders usually lead to a loss of independence for the patients and high costs for the health system (Stolze et al., 2005). Parkinson's disease is the most common movement disorder, a hypokinetic syndrome due to neurodegeneration of the substantia nigra. Dystonia, on the other hand, is a hyperkinetic disorder characterised by tonic and phasic involuntary muscle contractions. (Haegelen et al., 2013); (Kupsch et al., 2003) The symptoms associated to both diseases can be relieved or suppressed by a continuous pharmaceutical treatment. However, with long-term treatment some patients develop resistance to drugs and a surgical procedure may be required. In such cases, deep brain stimulation (DBS) is the common clinical procedure, promoting stimulation in target areas such as the subthalamic nucleus (STN) or the globus pallidus internus (GPi) (Haegelen et al., 2013). For the stereotactic implantation, optimal target site is chosen in relation to the midcommissural point, as described by Guridi et al., (2000). The motor and neuropsychological outcomes depend highly on the precise location and trajectory of the electrodes, which when stimulated will inhibit the activity in the target structures for each disease (Haegelen et al.,

2013); (Lozano et al., 2004).

However, due to possible shifts of DBS leads during surgical procedure, the final electrodes locations can be misaligned from the planned optimal target sites (Lalys et al., 2013); Videen T.O. et al., 2008). Therefore, it is vital to accurately locate the position of electrodes after DBS implantation, in order to avoid an undesirable stimulation of non-target areas.

In order to perform a detailed analysis of the final anatomical position of each electrode, several approaches were developed using multimodal techniques, combining anatomical and functional information (Hemm et al., 2009); (Lalys et al., 2010); (Bardinet et al., 2009). Such methods are indicated to confirm the implanted electrodes near the target basal ganglia structures and avoid the activation of the ones near others structures, which are known to promote acute side effects (Lozano et al., 2004). In addition, as described by Thani et al., (2011), an accurate anatomical location of each electrode is fundamental in quality control and to perform a more careful selection of the best stimulation parameters for DBS.

Nevertheless, the localisation of each DBS electrodes is still a challenging procedure. The presence of metal implants in MRI or CT scans,

such as the electrodes and wires of the DBS lead, can induce considerable image artefacts (Hebb et al., 2010). These image distortions limit the capacity to differentiate the electrodes from the DBS lead and therefore obtain their precise location.

In the literature, several techniques are referred to estimate the precise location of DBS electrodes.

Hebb et al., (2010) described an improvement in the visualization of DBS's electrodes by using a CT imaging with an extended Hounsfield unit (EHU) scale. Using EHU-CT each electrode can be clearly visualized without any special image processing techniques.

Since electrodes are indistinguishable from the DBS lead in the standard CT or MRI scans, some authors perform an electrodes artefact analysis, based on semiautomatic algorithms, to gathered information of the white and black artefacts dimensions, and correlated it with the exact location of the DBS electrodes. (Hemm et al., 2009); (Pollo et al., 2004). Lalys et al., (2013) described an automatic approach by focusing the electrode artefact analysis within a specific region, restricted by a brain mask. However, the accuracy of these methods are highly dependent on the area of signal artefact induced by the DBS lead (Thani et al., 2011).

On the other hand, the exact coordinates of each electrode can be estimated based on the detection of the lowest tip of the DBS lead and its trajectory (Rozanski et al., 2013); (Videen et al., 2008). These estimations are manually performed in a neuroimaging software by an experienced physician. As result, commissure ROIs are manually drawn in the coordinates previously estimated. However, this process is very time consuming, complex and requires an expert, with prior knowledge in neuroimaging software tools.

In this study, we propose a user-friendly system to automated segmentation and estimate the 3D position of each electrode from the DBS lead, implanted within the brain. Furthermore, a multimodal pipeline is presented to provide anatomical visualization of DBS electrodes, and therefore assist the neurologists in the confirmation of the implanted electrodes near the target areas.

2 MATERIALS

For this study 16 patients (eight with advanced Parkinson disease and eight with focal Dystonia) undergoing DBS were selected. All patients were informed and gave their consent. Stereotactic electrode insertion was carried out as previously described by Singh et al., (2011). Parkinson patients were operated in local anaesthesia to enable clinical outcome; dystonia patients were operated in general anaesthesia to avoid hyperkinetic movements during operation.

All the patients had electrodes implanted bilaterally. The DBS lead position was confirmed by post-operative CT or T2 scans. A pre-operative T1 with 0.98 x 0.98 x 1*mm* voxel size was acquired to guide the surgery and to visualize the target structure. The T1-MRI images were gathered by a 3T-MRI unit (Sigma Exite MD GE). CT scans were acquired by GE scanner, Brighspeed16 unit. For the implantation a quadripolar electrode array was used (model 3389, Medtronic Neurological Division, Minnesota, USA) with 4 electrodes at the tip, spaced 0.5mm apart delivering stimulation individually or in combination.

In Parkinson patients, DBS electrodes for continuous activation were chosen after intense testing for best clinical outcome according to UPDRS scale. In dystonia patients, lowest DBS electrodes were activated unless adverse effects occurred.

3 METHODS

In this section, we describe the multimodal pipeline for co-registration and the electrodes segmentation algorithm. Furthermore, the functionalities of the system are presented.

3.1 Multimodal Neuroimage Fusion

The skull-stripping tool BET (Brain extraction tool), available in FSL, was used in all dataset to remove the skull from the T1-MRI images.

Both CT and T2 images were co-registered using a linear affine transformation with 6 degrees of freedom. The geometric transformation was applied using FLIRT (FMRIB's linear image registration tool), accessible in FSL 5.0, with T1-MRI as reference image. Since the motion between images was not significant, the angular range over which the initial optimization search stage is performed was set between -30 to 30 for all the axes. The cost function chosen was the normalized mutual information, an entropy-based cost function widely used for inter-modal alignments, and described as the one with more accurate results for this type of images (Cahill, 2010).

3.2 DBS Electrodes Segmentation

For the segmentation of each DBS electrode, an algorithm was developed in MATLAB using the CT and T2 data co-registered with T1-MRI.

The algorithm automatically determines the bottom and upper tip of the DBS lead to deduce its trajectory. The coordinates of each electrode are estimated based on the DBS lead trajectory and the standard distances of each electrode to the bottom tip, provided in the datasheet of DBS lead.

In order to support the neurologists' task in the segmentation of the electrodes, a user interface was built to implement this algorithm, making this process more user-friendly.

The algorithm developed for the automatic segmentation of DBS electrodes is described below in more detail.

3.2.1 DBS Lead Segmentation

Initially, to determine the trajectory of the lead it is necessary to extract it from the data and identify its bottom and upper tips.

Since intensity-based segmentation approaches were incapable to eliminate completely the skull in the CT and T2 data, due to intensity similarities between the DBS lead and the skull, a 3D labelling connected components algorithm was designed. The algorithm principle is based on the evidence that the position of the lead varies slightly from slice to slice.

Thus, the algorithm estimates the centroid of each label of each binary image, which is obtained by a thresholding operation. The closest centroids in successive slices are connected and a Euclidean distance threshold is applied to eliminate the 3D centroids combinations which are far apart and therefore cannot represent the DBS lead. A connectivity recursive function was designed to set up 3D connect components, each one with a different label assigned, based on the information of the centroids connection between slices. Since each centroid was constrained to be connected to only one centroid in the following slice, no centroids were repeated in different 3D connected components. The recursive function ends the set-up of each connected component when a centroid has no connection with any centroids on the following slice. When all the centroids have a 3D label assigned, the recursive function cease.

The 3D labels of DBS leads are automatically selected since they are the ones localized along a trajectory from surface to deep brain. The bottom tip is defined in the deepest slice in which the DBS label is visible, and the upper tip in the last slice.

3.2.2 Electrodes Position Estimation

In order to determine each position of the electrode, the x, y and z voxel coordinates of the bottom and upper tips of the DBS lead were transformed to *mm* space by equation 1, 2 and 3. For the transformation between coordinate spaces, it was used a 4*x*4 affine transformation matrix, *M*, saved in the header of the NIfTI file.

$$x_{mm} = [x \quad y \quad z]_{voxel} \times M'_{1,j-1} + M_{1,4} \qquad (1)$$

$$y_{mm} = [x \quad y \quad z]_{voxel} \times M'_{2,j-1} + M_{2,4} \qquad (2)$$

$$z_{mm} = [x \quad y \quad z]_{voxel} \times M'_{3,j-1} + M_{3,4} \qquad (3)$$

$$x_{voxel} = [x \quad y \quad z]_{mm} \times \left(M^{-1}_{1,j-1}\right)' + M^{-1}_{1,4} \qquad (4)$$

$$y_{voxel} = [x \quad y \quad z]_{mm} \times \left(M^{-1}_{2,j-1}\right)' + M^{-1}_{2,4} \qquad (5)$$

$$z_{voxel} = [x \quad y \quad z]_{mm} \times \left(M^{-1}_{3,j-1}\right)' + M^{-1}_{3,4} \qquad (6)$$

Using the *mm* coordinates of DBS's tips, it was performed the following trigonometric equations, as illustrated in Figure 1 (A).

$$\alpha = \tan^{-1} \frac{\delta y}{\delta x} \qquad (7)$$

$$d = \frac{\delta x}{\cos \alpha} \qquad (8)$$

$$\beta = \tan^{-1} \frac{h}{d} \qquad (9)$$

$$H = \frac{d}{\cos \beta} \qquad (10)$$

$$\varphi = \cos^{-1} \frac{h}{H} \qquad (11)$$

Knowing the values of these variables and the distance of each electrode to the bottom tip, it was possible to calculate the *mm* coordinates of the centre of each electrode, $\delta x1$, $\delta y1$, $h1$, by trigonometric relations as illustrated in Figure 1 (B).

The obtained positions were transformed to the voxel space by equation 4, 5 and 6, to set up the 3D electrodes mask.
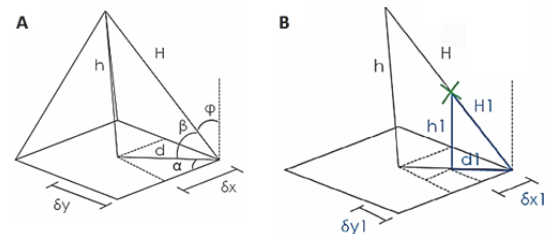

Figure 1: (A) 3D representation of the relationship between the lengths and angles for the different sides of the DBS lead, where H represents its trajectory. (B) 3D representation of the distances of a figurative electrode in relation to the bottom tip.

3.3 User-friendly Interface

The workflows of the algorithms described above were implemented in an interface, developed in MATLAB, which automatically estimates the bottom and upper tips of the DBS lead and calculates, using the trigonometric relations, each position of the electrodes.

With the help of this system, the user can automatically export a 3D mask with only electrodes information, i.e., without brain, beam hardening and skull information. Furthermore, the user can obtain 3D masks of the DBS leads as well as specify which electrodes will be in the mask to be exported.

Since the CT or T2 datasets were aligned with T1-MRI, before the segmentation, the interface allows the overlapping of the T1-MRI with the electrodes or DBS masks. This functionality is useful to support the interpretation of data by the neurologists.
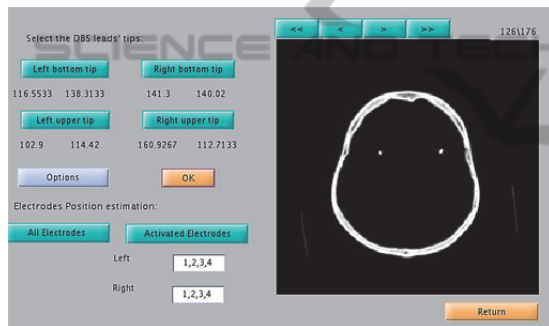

Figure 2: Workflow Interface window for semiautomatic segmentation, in which the user presses in the lateral buttons to select the DBS's tips, using the cursor.

An options panel was added to change default parameters and therefore optimize the DBS segmentation process or even change the specifications of the DBS lead, such as the distances of each electrode in relation to the bottom tip. This latter feature is essential in case other DBS model, different from the default, is used.

In case the user does not agree with the suggestions given by the automatic approach, there is the possibility of manual change (in the options panel) of some segmentation parameters or even the opportunity to perform a semiautomatic segmentation, as depicted in Figure 2. This latter only performs the pipeline using the trigonometric relations, where the bottom and upper tips are manually selected by the user.

In addition, the dataset can be analysed by passing the slices, which can be helpful when the automatic approach is selected to confirm the slices

where the DBS tips appear.

4 RESULTS AND DISCUSSION

4.1 Multimodal Neuroimage Fusion

Figure 3 revealed a fine alignment between T1 and T2 or CT images. Therefore, the parameters chosen for the co-registration are recommended for inter-modal alignments, linear affine transformations and datasets in which the motion is not significant.

According to Jenkinson et al., (2001), the use of FLIRT in the presence of large ventricles, may result in misalignments for others structures. In these cases, higher order transformations or non-linear warpings may be used to achieve fine alignments.
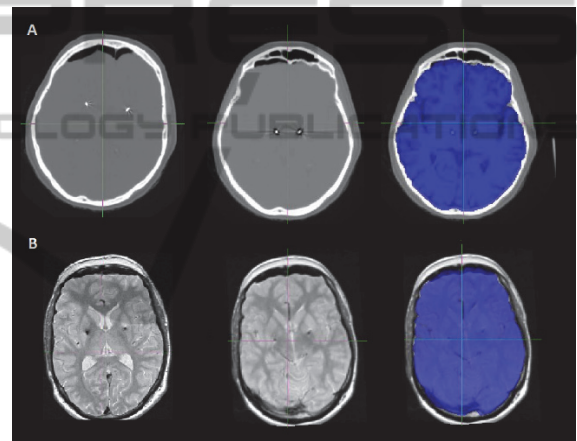

Figure 3: Co-registration of (A) CT with T1 datasets and (B) T2 with T1 datasets. (Left) Original CT and T2 images; (Center) CT and T2 images aligned with T1 using FLIRT; (Right) Fusion of CT or T2 images with T1, which is displayed in blue.

Although the patients of this study were elderly and therefore more susceptible to present large ventricles, no failures were seen in FLIRT performance, using the multimodal pipeline described in this study.

4.2 DBS Electrodes Segmentation

As depicted in figure 4 (A), 3D labeling connected components algorithm was very efficient to produce a mask with only DBS lead data, for the CT datasets. Nevertheless, the algorithm does appear to fail on automatic mode for T2 datasets. Therefore to generate the electrodes masks with T2 data, it is recommended to use the semiautomatic segmentation approach.

The electrodes position estimated by MATLAB and the ones deduced manually by a physician were compared in order to validate the MATLAB interface and algorithm. The manually localization of electrodes position was performed as described by Rozanski et al., (2013).

Table 1: The mean ($\bar{x}$) and standard deviation (σ) of the absolute differences, in *mm*, estimated from all datasets, regardless of the segmentation method used for the electrodes mask establishment.

mm	*x*	*y*	*z*
$\bar{x}$	0,507	0,592	0,444
σ	0,337	0,426	0,366

Table 2: The mean ($\bar{x}$) and standard deviation (σ) of the absolute differences, in mm, estimated with the automatic and semiautomatic method.

mm	Semiautomatic			Automatic		
	x	y	z	x	y	z
$\bar{x}$	0,581	0,557	0,359	0,385	0,678	0,587
σ	0,362	0,358	0,316	0,258	0,530	0,413

Table 1 shows the average of the differences in *mm* between the coordinates of each electrode obtained by the interface and the ones manually deduced, for the three axis. These differences are very small, as suggested by Table 1.

Through the analysis of Table 2, it is concluded that semiautomatic segmentation was less precise in x direction compared with the automatic method, probably due to random errors introduced by the user in the selection of the tips and systematic errors due to the voxel resolution, restricting the selection of the center of the tips by the cursor. On the other hand, automatic segmentation was less precise in y and z directions, probably due to the presence of some beam hardening in the upper slices that may have affected the calculation of the centroid of the upper tip and therefore the estimation of DBS's trajectory.

However, the trajectory imprecisions are not significant, since either using the semiautomatic or the automatic approach (Table 2), the differences found were less than a voxel size.

Regarding computational time, the creation of the electrodes mask using our tool lasts around 1 minute, which when compared with the normal manual procedure performed by the physicians that lasts around 40 min, is much faster and practical.
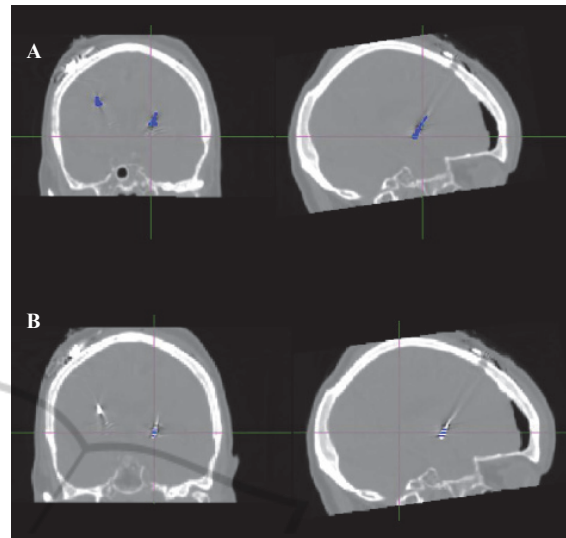

Figure 4: Fusion of CT images pre-aligned with: (A) the DBS lead mask obtained after the 3D labelling connect components algorithm; (B) electrodes mask obtained by the automatic algorithm.

Normally, the physician needs to have prior knowledge on neuroimaging software to manually determine the bottom tip and specific angles in relation to the DBS lead, in order to estimate its trajectory and therefore determine each location of the electrodes (Rozanski et al., 2013); (Guo et al., 2013). Videen et al., (2008) uses a similar approach by manually estimate the deepest tip and the center of the lead in upper slices. On the other hand, Zonenshayn et al., (2004) calculates the stereotactic frame's arc, collar angles and the most distal electrode in stereotactic space by microelectrode recordings, in order to estimate the trajectory of the lead. In both methods, based on the trajectory and the bottom tip, the coordinates of each electrode are manually determined and used to create ROIs. This entire procedure is very time consuming when compared with the segmentation time of our tool, which makes our system more pragmatic and motivating for neurologists.

Therefore, our interface can be widely used by physicians, since it is not time consuming and allows an automatic and accurate estimation of electrodes locations.

Furthermore, the user-friendly interface allows the user to export a mask with DBS leads as well as specify which electrodes will be in the mask to be exported. These characteristics allow, for instance, the selection of only the activated ones, which can be useful in DBS investigation studies. As opposed, the entire DBS lead mask can be useful in a clinical environment to study the impact of microlesional

damage caused by its implantation in the brain (Horn et al., 2013).

The co-registration pipeline and the electrodes masks exported by the interface allow the fusion of T1-MRI with electrodes in a single view, as depicted in Figure 5. This is important to visualize the anatomical electrodes position and confirm their implantation in the target areas, activating only the ones which may lead to the better outcomes and avoiding the ones which are near to structures such as the substantia nigra responsible to promote acute side effects (Ulla et al., 2011).
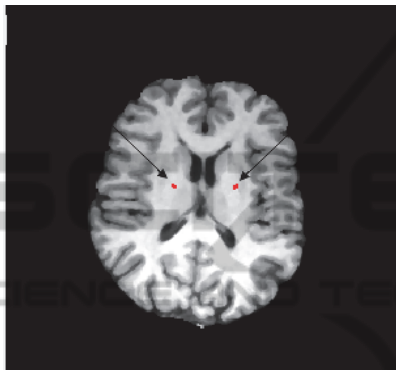

Figure 5: Multimodal neuroimage fusion: Electrodes mask (red) overlaid with T1-MRI dataset where adjacent deep brain structures can be related to the electrode positioning.

5 CONCLUSIONS

The purpose of this study was to develop a system for the localization of electrodes from the DBS lead and use multimodal techniques to confirm their placement in the neurosurgery target areas.

Since the multimodal co-registration pipeline results in fine alignments and an accurate brain extraction (for all 16 cases), the parameters chosen either for BET and FLIRT are recommended to visualize the anatomic position of DBS electrodes, in future studies.

Regarding the electrodes segmentation and localization, it can be concluded that the user-friendly interface can be useful in a clinical environment and in future DBS studies to automatically produce the electrodes masks, since the differences between the detected electrodes positions and the ones estimated manually by an experienced physician were less than a voxel in all cases.

In addition, the creation of the electrodes mask using our tool lasts around 1 minute, much faster and practical when compared with the common

procedures performed by physicians.

Therefore, using our system it is possible to obtain an anatomic location of each electrode and may contribute to the improvement of the efficacy of DBS and consequently the patient's outcome.

In the future, it would be interesting to use the system to find any correlation of the exact anatomic position of the electrodes with the clinical outcomes. In additon, using DTI information, it would be also possible to study the influence of the 3D electrode localisation in the connectivity patterns of the cortico-basal-ganglia-thalamo-cortical circuit. These studies could be extended not only for Parkinson and Dystonia patients, but for all the diseases treated by DBS such as resistant depression, schizophrenia and mood disorders.

ACKNOWLEDGEMENTS

REFERENCES

Bardinet E., Bhattacharjee M., Dormont D., Pidoux B., Malandain G., Schüpbach M., Ayache N., Cornu P., Agid Y., Yelnik J., 2009. A three-dimensional histological atlas of the human basal ganglia. II. Atlas deformation strategy and evaluation in deep brain stimulation for Parkinson disease. *J Neurosurg.,* 110(2):208-219.

Cahill N. D., 2010. Normalized measures of mutual information with general definitions of entropy for multimodal image registration. In *WBIR'10 Proceedings of the 4th international conference on Biomedical image registration*, pages 258-268. Springer-Verlag.

Guo S., Zhuang P., Hallett M., Zheng Z., Zhang Y., Li J., Li Y., 2013. Subthalamic deep brain stimulation for Parkinson's disease: correlation between locations of oscillatory activity and optimal site of stimulation. *Parkinsonism Relat Disord.*, 19 (1):109-14.

Guridi J., Rodriguez-Oroz M. C., Lozano A. M., Moro E., Albanese A., Nuttin B., Gybels J., Ramos E., Obeso J. A., 2000. Targeting the basal ganglia for deep brain stimulation in Parkinson's disease. *Neurology*, 55(12 Suppl 6):S21-8.

Haegelen C., Coupé P., Fonov V., Guizard N., Jannin P., Morandi X., Collins D. L., 2013. Automated segmentation of basal ganglia and deep brain structures in MRI of Parkinson's disease. *Int J Comput Assist Radiol Surg*, 8(1):99-110.

Hebb A. O., Miller K. J., 2010. Semi-automatic stereotactic coordinate identification algorithm for routine localization of Deep Brain Stimulation electrodes. *J Neurosci Methods*, 187(1):114-9.

Hemm S., Coste J., Gabrillargues J., Ouchchane L., Sarry L., Caire F., Vassal F., Nuti C., Derost P., Durif F., Lemaire J. J., 2009 Contact position analysis of deep brain stimulation electrodes on post-operative CT images. *Acta Neurochir (Wien),* 151(7):823-9.

Horn A., Schönecker T., Schneider G-H., Kühn A. A., 2013. Automatic reconstruction of DBS-Electrode Placement from post-operative MRI-images. *Journal of Neural Transmission,* 120:1137-1159.

Jenkinson M., Smith S., 2001. A global optimisation method for robust affine registration of brain images. *Med Image Anal.*, 5(2):143-56.

Kupsch A., Kuehn A., Klaffke S., Meissner W., Harnack D., Winter C., Haelbig T. D., Kivi A., Arnold G., Einhäupl K. M., Schneider G. H., Trottenberg T., 2003. Deep brain stimulation in Dystonia. *J Neurol* 250 [Suppl 1]: I/47–I/52.

Lalys F, Haegelen C, Ferre JC, El-Ganaoui O, Jannin P., 2010. Construction and assessment of a 3-T MRI brain template. *Neuroimage*, 49(1):345-354.

Lalys F., Haegelen C., D'albis T., Jannin P., 2013. Analysis of electrode deformations in deep brain stimulation surgery. *Int J Comput Assist Radiol Surg.*

Lozano A. M., Mahant N., 2004. Deep brain stimulation surgery for Parkinson's disease: mechanisms and consequences. *Parkinsonism Relat Disord*, 10, Suppl 1:S49-57.

Pollo C., Villemure J.G., Vingerhoets F., Ghika J., Maeder P., Meuli R., 2004. Magnetic resonance artifact induced by the electrode Activa 3389: an in vitro and in vivo study. *Acta Neurochir (Wien)*, 146(2):161-4.

Rozanski V. E., Vollmar C., Cunha J. P., Tafula S. M. N., A. S.-A., Patzig M., Mehrkens J. H., Bötzel K., 2013. Connectivity patterns of pallidal DBS electrodes in focal Dystonia: a diffusion tensor tractography study. *Neuroimage,* 84: 435–442.

Singh A., Kammermeier S., Mehrkens J. H., Bötzel K., 2012. Movement kinematic after deep brain stimulation associated microlesions. *J. Neurol Neurosurg Psychiatry*, 83(10):1022-6.

Stolze H., Klebe S., Baecker C., Zechlin C., Friege L., Pohle S., Deuschl G., 2005. Prevalence of gait disorders in hospitalized neurological patients. *Movement Disorders*, 20(1):89-94.

Thani N. B., Bala A., Swann G. B., Lind C. R., 2011. Accuracy of postoperative computed tomography and magnetic resonance image fusion for assessing deep brain stimulation electrodes. *Neurosurgery*, 69(1):207-14.

Ulla M., Thobois S., Llorca P. M., Derost P., Lemaire J. J., Chereau-Boudet I., de Chazeron I., Schmitt A.,

Ballanger B., Broussolle E., Durif F., 2011. Contact dependent reproducible hypomania induced by deep brain stimulation in Parkinson's disease: clinical, anatomical and functional imaging study. *J Neurol Neurosurg Psychiatry*, 82(6):607-14.

Videen T. O., Campbell M. C., Tabbal S. D., Karimi M., Hershey T., Perlmutter J. S., 2008. Validation of a fiducial-based atlas localization method for deep brain stimulation contacts in the area of the subthalamic nucleus. *Journal of Neuroscience Methods,* 168:275–281.

Zonenshayn M., Sterio D, Kelly P. J., Rezai A. R., Beric A., 2004. Location of the active contact within the subthalamic nucleus (STN) in the treatment of idiopathic Parkinson's disease. *Surg Neurol.*, 62(3):216-25.